METEOROLOGICAL APPLICATIONS
Meteorol. Appl. **14**: 195–203 (2007)
Published online in Wiley InterScience
(www.interscience.wiley.com) DOI: 10.1002/met.22

RMetS
ROYAL METEOROLOGICAL SOCIETY

Bias adjustment and long-term verification of radar-based precipitation estimates

Iwan Holleman*
Royal Netherlands Meteorological Institute (KNMI), The Netherlands

ABSTRACT: Quantitative precipitation estimates (QPE) based on weather radar observations are used more and more for water management, in numerical weather prediction models, and for monitoring of severe weather. A straightforward method for bias adjustment of radar-based and hourly-updated precipitation accumulations is described. In addition a long-term verification of the bias-adjusted composites over a six year period using dependent and independent gauge data is presented. It is found that the adjustment scheme effectively removes the mean-field bias from the raw accumulations. The adjustment method cannot correct for a range-dependent bias and therefore it is recommended to also use a simple vertical profile of reflectivity (VPR) adjustment procedure. Copyright © 2007 Royal Meteorological Society

KEY WORDS radar; bias adjustment; QPE; hourly; verification

Received 9 January 2007; Revised 5 April 2007; Accepted 17 April 2007

1. Introduction

Quantitative precipitation estimates (QPEs) on high spatial and temporal resolutions, i.e. in the order of kilometres and hours, are of increasing importance for operational water management, assimilation in and verification of numerical weather prediction (NWP) models, monitoring of severe weather, and issuing local warnings. An operational weather radar or, better, a network thereof, can routinely provide this kind of information. In a recently finished European COST (Cooperation in the field of Scientific and Technical research) action the use of radar observations in hydrological and NWP models has been assessed (Rossa *et al*., 2005).

Quantitative use of weather radar precipitation estimates is not straightforward due to a variety of gross errors affecting the observations (Wilson and Brandes, 1979; Joss and Waldvogel, 1990). For C-band radars at mid-latitudes, the most important ones are non-uniform vertical profile of reflectivity (VPR), variability of the drop size distribution (DSD), and attenuation due to strong precipitation intensity. At longer ranges the height of observation will increase and in the presence of a significant VPR gradient this will typically result in an underestimation of the accumulated precipitation (Joss and Waldvogel, 1990; Koistinen, 1991). VPR can be estimated using climatological profiles, mean reflectivity profiles or local profiles obtained at short ranges (Vignal *et al*., 2000; Vignal and Krajewski, 2001; Koistinen *et al*., 2003). Alternatively, it can be determined using a sophisticated technique based on inverse theory (Andrieu and Creutin, 1995a; Vignal *et al*., l999) or using information from an NWP model (Michelson *et al*., 2005). In a flat country, application of sophisticated VPR adjustment may be overdone because at 150 km range only a translation from 2 km altitude down to ground level is needed, which is actually within the radar beam width. A straightforward technique for VPR adjustment based on the analysis of accumulated precipitation data at two different altitudes has been proposed by Holleman (2004).

The translation of radar reflectivity Z into rainfall intensity R is non-trivial and depends heavily on the actual drop size distribution (DSD). The most famous publication on this subject 'The Distribution of Raindrops with Size' by Marshall and Palmer (1948) is almost 60 years old. Uijlenhoet and Stricker (1999) have investigated the inconsistency of the Z-R relations in great detail and have developed a consistent rainfall parameterization. Attenuation of the radar beam causes underestimation of the precipitation intensity or even disappearance of the rain cells behind very strong cells. A correction algorithm for attenuation is potentially highly unstable (Hitschfeld and Bordon, 1954) as confirmed by studies using C-band and X-band radars (Delrieu *et al*., 1999; Berne and Uijlenhoet, 2006).

A mean-field bias adjustment algorithm can be used to reduce the gross errors in radar-based precipitation estimates. Wilson (1970) pioneered with the integration of radar and raingauge data and showed that this can improve the area rainfall measurements. A real-time calibration of radar-based surface rainfall estimates by telemetering raingauges was performed by Collier (1983, 1986a,b) and an improved accuracy was seen on most locations within 75 km of the radar site. Nowadays mean

* Correspondence to: Iwan Holleman, Royal Netherlands Meteorological Institute, NL-3730AE De Bilt, Netherlands.
E-mail: holleman@knmi.nl

field bias adjustment of radar-based quantitative precipitation estimates is widely used. (Fulton *et al*., 1998; Harrison *et al*., 2000; Borga *et al*., 2002; Chumchean *et al*., 2006).

Here we present a straightforward method for bias adjustment of accumulated precipitation composites. The method is used operationally at the Royal Netherlands Meteorological Institute (KNMI) for an hourly-updated QPE product. In addition, an extensive spatial and temporal verification of the bias-adjusted composites over a 6 year period (2000–2005) using dependent and independent gauge data is presented. It is found that the real-time adjustment scheme effectively removes the mean-field bias from the raw accumulations over a large area and that it substantially reduces the daily standard deviation. The adjustment method cannot correct for a range-dependent bias and it is recommended to use a simple VPR adjustment procedure for that.

2. Radar and gauge data

KNMI operates two identical C-band Doppler weather radars from SELEX, formerly known as Gematronik. The De Bilt radar is located at a latitude of 52.10°N and a longitude of 5.18°E. The Den Helder radar is located at a latitude of 52.96°N and a longitude of 4.79°E. The locations of the weather radars and the extent of the 165 km range circles are displayed in Figure 1. The received signal is digested by a RVP6 radar processor (Sigmet, 1998) and the generation of products is done using Rainbow 3.4 software (Gematronik, 2003). The operational reflectivity scan for precipitation estimation consists of a four elevation scan (0.3, 1.1, 2.0, and 3.0 degrees) which is performed every 5 min. From these three-dimensional scans pseudoCAPPI images, i.e. horizontal cross sections of reflectivity at constant altitude, are produced with a target height of 800 m above antenna level and a horizontal resolution of 2.4 km. Ground clutter and anomalous propagation clutter are removed from these images using a stepwise procedure described in Wessels and Beekhuis (1994).

Two independent networks for the observation of precipitation depth at different temporal and spatial resolutions are deployed by KNMI. The climatological network is a dense network (one station per 100 km^2) of about 325 volunteers who report the accumulated precipitation daily at 0800 UTC using manual precipitation gauges. These conventional gauges consist of a funnel with a horizontal entry area of 0.02 m^2 and a collection reservoir. The automatic weather station (AWS) network of KNMI is a network of 35 stations which report every 10 min a number of meteorological quantities, amongst others temperature, dewpoint, wind speed and direction, cloud base and cover, and precipitation depth. The automatic rain gauges determine the amount of precipitation by measuring the position of a floater placed in a measuring cell. Figure 1 shows two maps of The Netherlands with the locations of the manual and automatic rain gauges.

3. Generation of Bias-Adjusted Accumulation Composites

3.1. Accumulation

Before accumulation the radar reflectivity values are converted to rainfall intensities using a fixed 'Marshall–Palmer type' Z-R relationship (Marshall and Palmer, 1948; Marshall *et al*., 1955):

$$Z = 200R^{1.6} \tag{1}$$

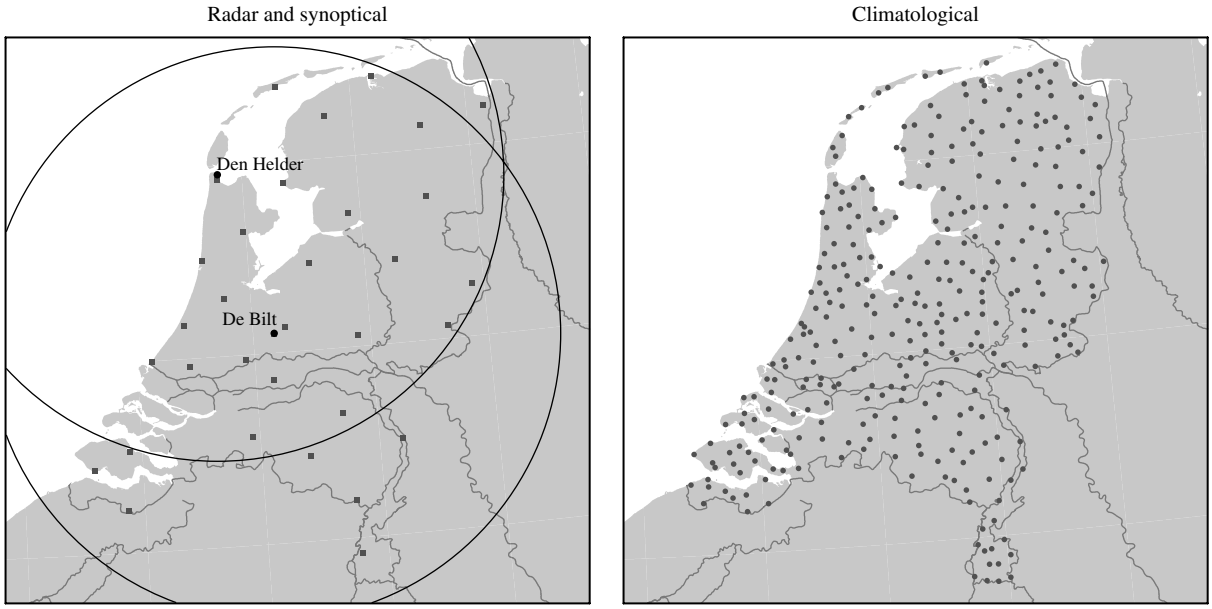

Figure 1. The left map shows the KNMI weather radars (2) and the national synoptical network with the automatic precipitation gauges (35) and the right map shows the KNMI climatological network of manual precipitation gauges (325). The weather radars are indicated with filled circles and the 165 km range circles are plotted as well.

DOI: 10.1002/met

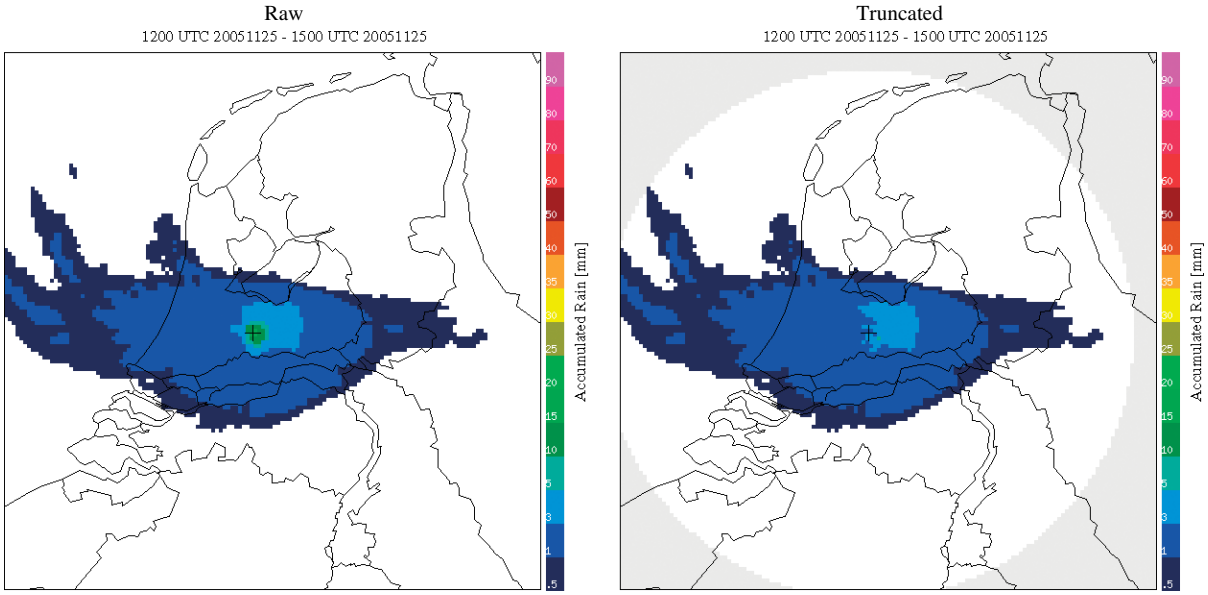

Figure 2. Raw (left) and truncated (right) accumulated precipitation products from the radar in De Bilt between 1200 and 1500 UTC on 25 November 2005. The images have been zoomed to show better the relevant area around The Netherlands.

with the radar reflectivity Z in mm^6/m^3 and rainfall rate R in mm/h. To avoid the accumulation of noise, radar reflectivities below 7 dBZ (0.1 mm h^{-1}) are not accumulated. Similarly, the impact of large hail and residual strong clutter on the precipitation estimates is suppressed by maximizing the reflectivity to 55 dBZ (100 mm h^{-1}). On the basis of the 5-min reflectivity products, running 3-h accumulations are calculated every hour. A 5-point median filter is applied to the accumulated precipitation products to reject local outliers due to accumulated residual (ground) clutter. An example of a 'raw' accumulated precipitation product from the De Bilt radar for an extreme winter storm case on 25 November 2005 is displayed in the left image of Figure 2.

3.2. Truncation

From the example accumulation shown in the left image of Figure 2 it is evident that the largest precipitation depths are observed close to the radar in De Bilt (location marked by the cross). Figure 3 shows the mean accumulated precipitation as a function of range from the radar in De Bilt for the same case. Data are shown for the full operational range of the KNMI weather radars, i.e. 320 km. The observed accumulated precipitation has been averaged in azimuthal direction. From the solid and dashed black curves in the figure, it is evident that the raw accumulation exhibits a sharp maximum (>15 mm) at short range from the radar (<15 km). This artifact is caused by accumulation of spurious echoes at short range from the radar. These spurious echoes mainly originate from transmitter noise and sidelobe clutter.

The mean-field bias correction method cannot correct for these spurious echoes at short ranges and therefore a truncation procedure has been developed to reduce the impact of these echoes. Within a predefined range from the radar, by default 15 km, the azimuthal-mean accumulation is calculated at 1 km intervals. When the azimuthal-mean accumulation is higher than that at the predefined range, the corresponding pixel values are rescaled such that the mean accumulation becomes equal to that at the predefined range. The effect of this truncation on the mean accumulation as a function of range is depicted by the shifted solid curve in Figure 3. The maximum range has been set to 165 km which is just enough to cover The Netherlands with the two operational weather radars. Figure 2 shows the raw (left image) and truncated (right image) accumulation products.

3.3. Bias adjustment

A mean-field bias adjustment algorithm is used to reduce the gross error in the truncated 3-h precipitation

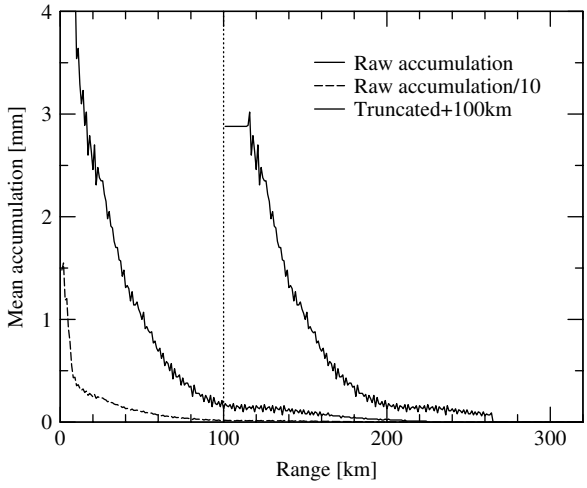

Figure 3. Mean accumulated precipitation as a function of range from the radar in De Bilt between 1200 and 1500 UTC on 25 November 2005 (Figure 2). The observed precipitation has been averaged in azimuthal direction.

DOI: 10.1002/met

accumulations as observed against the automatic rain gauge observations. The bias-adjusted precipitation estimates are calculated hourly from the uncorrected, i.e. truncated, precipitation estimates:

$$\tilde{R}(i, j) \equiv \frac{R(i, j)}{F} \tag{2}$$

where $\tilde{R}(i, j)$ and $R(i, j)$ represent the bias-adjusted accumulation and uncorrected accumulation, respectively, of the pixel at image coordinates (i, j). Assume that for a certain accumulation period, an uncorrected radar accumulation product $R(i, j)$ and observations from a number of rain gauges G_n are available. An equation for the bias-adjustment factor F can be derived from the requirement that the mean-field bias should be zero after adjustment ($B = 0$):

$$B \equiv \frac{1}{N} \sum_{n=1}^{N} \left[\frac{R(i_n, j_n)}{F} - G_n \right] = 0 \tag{3}$$

where (i_n, j_n) are the image coordinates of rain gauge n and N is the number of available rain gauges. By rearrangement one finds the following equation for the bias-adjustment factor:

$$F = \frac{\sum_{n=1}^{N} R(i_n, j_n)}{\sum_{n=1}^{N} G_n} \tag{4}$$

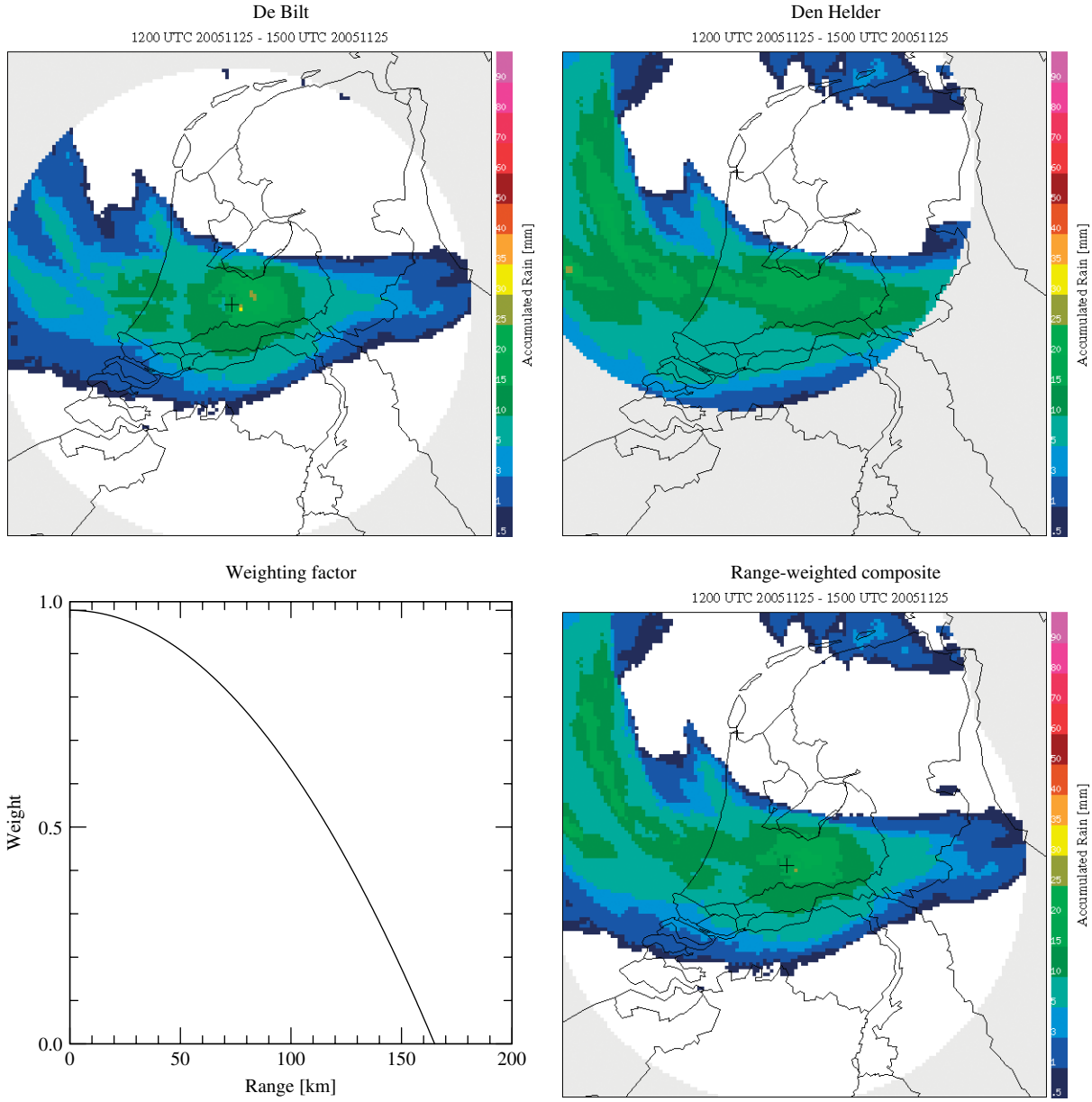

Figure 4. Example of bias-adjusted precipitation accumulation products from the radars in De Bilt (upper-left) and Den Helder (upper-right) for 1500 UTC on 25 November 2005. The lower-left frame of the figure displays the weighting factor as a function of range as used for the composites. The lower-right image shows the range-weighted composite of the bias adjusted accumulations from both radars.

DOI: 10.1002/met

where basically the total amount of precipitation in the radar image and in the rain gauge network are matched. The bias-adjustment factor is only calculated when the numerator and denominator are not too close to zero (>5 mm), and else it is set to unity. When presenting a distribution of obtained bias-adjustment factors it is often beneficial to make them more symmetrical by using a decibel-scale:

$$\tilde{F}[\mathrm{dB}] \equiv 10 \cdot^{10} \log F \tag{5}$$

and thus a neutral adjustment factor (unity) corresponds to 0 dB.

3.4. Compositing of accumulations

The operational bias-adjusted accumulation product will be composed of the accumulation products from the individual weather radars. Before compositing, the accumulation products from the different radars must be reprojected to a common geographical projection (see upper images of Figure 4). The question remains how to combine the pixel values, e.g. maximum or mean, from different radars in the overlapping regions. A range-weighted mean of the available pixel values in the composite product is used. In both maximum and mean composites, discontinuities at the edge of the coverage of a radar sometimes occur. A range-weighted mean where the weight of the radar data gradually decreases with increasing range can be used to suppress these discontinuities.

The lower-left frame of Figure 4 displays the weighting factor as a function of range from the weather radar as used for the range-weighted composites. The weighting factor as a function of range $W(r)$ is calculated from:

$$W(r) = \begin{cases} 1 - \left(\frac{r}{R_x}\right)^2 & \text{if} \quad r \le R_x \\ 0 & \text{if} \quad r > R_x \end{cases} \tag{6}$$

where R_x represents the maximum quantitative range (165 km). The data quality as a function of radar range is approximated by a quadratic function taking into account the increasing height and volume of the radar beam with increasing range.

A range-weighted composite of bias-adjusted precipitation accumulation products from the weather radars in De Bilt and Den Helder is shown in the lower-right image of Figure 4. The composite is built from the accumulation products of the individual radars as shown in the upper images of the figure. It is evident that in the range-weighted composite a smooth transition between the two radars is made.

4. Verification of bias-adjusted composites

A dataset containing 6 years (2000–2005) of weather radar accumulations and rain gauge observations has been used for a long-term evaluation of the bias-adjustment algorithm.

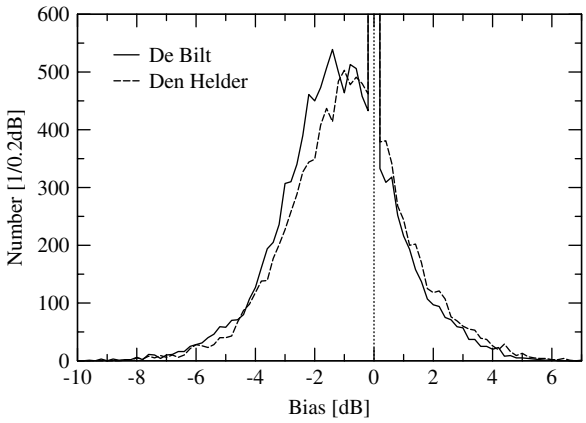

Figure 5. Histograms with the distribution of the bias-adjustment factors for the radars in De Bilt (solid curve) and Den Helder (dashed curve). The 6-year dataset (2000–2005) of bias-adjusted 3-h precipitation accumulations has been used for this figure. The histograms are constructed using a bin size of 0.2 dB. The off-scale peak at 0 dB reaches values of 41 320 and 42 094 for De Bilt and Den Helder, respectively.

4.1. Bias-adjustment factors per radar

Figure 5 shows two histograms with the distribution of the bias-adjustment factors for the radars in De Bilt and Den Helder. The off-scale peak at 0 dB, i.e. no adjustment, reaches to 41 320 and 42 094 for De Bilt and Den Helder, respectively. Taking into account the number of available accumulation products, it is seen that an adjustment is performed on about 20% of the products. It is evident from Figure 5 that the long-term distribution (6 years) of bias-adjustment factors is rather similar for De Bilt and Den Helder. The distribution is rather broad with a full width at half maximum of about 4 dB and it is shifted towards negative dB-values. The latter indicates that the weather radars are underestimating the precipitation depths on average. The mean underestimation is due to a climatological VPR which is decreasing with altitude.

The distribution for De Bilt in Figure 5 is shifted to slightly more negative values suggesting that the underestimation by this radar is somewhat stronger. A scatter and contour plot with the bias-adjustment factors of De Bilt and Den Helder is shown in Figure 6. Only pairs where both bias-adjustment factors are not equal to 0 dB are plotted. The geographical coverages of both radars are overlapping to a large extent (Figure 1). If the observed biases are primarily due to meteorological phenomena, a good correlation between the biases of both radars should be found. A reasonably good correlation between the bias-adjustment factors of both radars is evident from the figure. A correlation coefficient of $r = 0.76$ is found for the 6-year period. The majority of the pairs shows up above the $y = x$ diagonal because the bias of De Bilt is on average more negative than the bias of Den Helder (difference about 0.4 dB). This difference

DOI: 10.1002/met

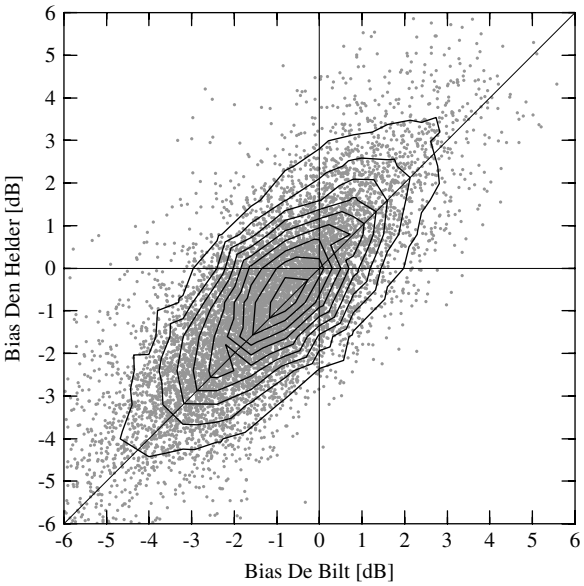

Figure 6. This scatter and contour plot shows the correlation between the bias-adjustment factor for the De Bilt radar and that for the Den Helder radar. Only pairs where both bias factors are not equal to 0 dB have been plotted. The contours are based on the scatter point density. The contour line interval and the inner contour correspond to 0.1 and 0.9 times the maximum density, respectively.

may be due to a calibration difference but could also be caused by the larger fraction of land surface covered by the De Bilt radar.

4.2. Verification against dependent gauges

The bias-adjusted composites of accumulated precipitation have been verified against observations from the automatic rain gauge network and the climatological rain gauge network. Because the former network has been used for the bias adjustment of the radar accumulations, this 'dependent' verification provides a health-check of the bias-adjustment procedure. The latter network enables a truly independent verification of the bias-adjusted composites. To enable the quantitative verification against the independent climatological rain gauge network, the 3-h accumulation products have been aggregated into 24-h accumulations running from 0800 to 0800 UTC. Only days where both weather radars have contributed at least 280 (out of maximum 288) 5-min reflectivity products to the accumulation product are included in the verification.

In Figure 7 scatter and contour plots of the raw accumulations (left frame) and the adjusted accumulations (right frame) against the automatic gauge observations are shown. For the raw accumulation product against the automatic gauge observations a major underestimation of the precipitation depths is seen. About one-third (10 313 out of 33 453) of the points lies above the dashed diagonal ($y = x$ identity line). The plot of the bias-adjusted accumulations looks quite different. The distribution of points below and above the identity line is approximately fifty-fifty, i.e. 15 715 points out of 33 124 lie above this line. In addition, the points appear evenly scattered around the identity line.

Table I lists the mean daily precipitation depth, the bias, and the standard deviation from the adjusted and raw accumulation products for all years in the verification dataset. The bias and standard deviation have been calculated using the automatic rain gauge observations. For the raw accumulations, a serious bias of roughly 40% of the mean precipitation depth is seen for all years. The standard deviation is substantially larger than the mean precipitation depth. It is evident that no significant

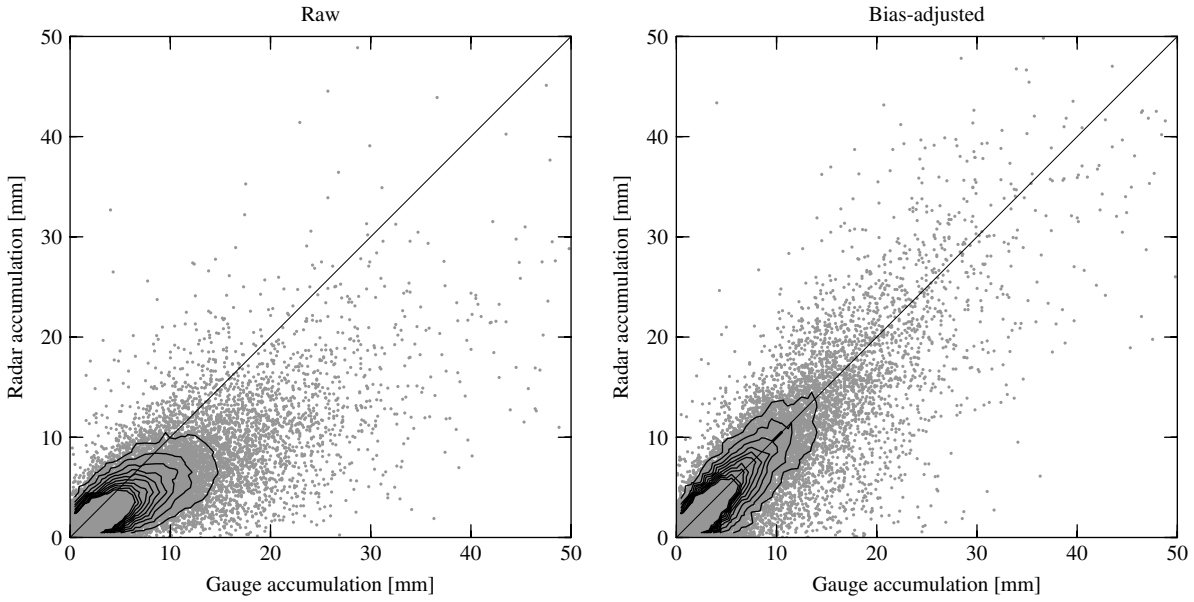

Figure 7. Scatter and contour plot of the adjusted (right frame) and raw (left frame) radar accumulations against the collocated gauge observations. The observations from the automatic rain gauge network have been used. The 3-h accumulation products have been aggregated into 24-h accumulation (0800–0800 UTC). The contours are based on the scatter point density. The contour line interval and the inner contour correspond to 0.01 and 0.1 times the maximum density respectively.

DOI: 10.1002/met

Table I. Verification results for adjusted and raw accumulation composites against the dependent dataset. The mean daily precipitation depth, bias and standard deviation are listed in mm. The number of gauge observations used for the verification is listed as well.

	Adjusted				Raw		
Year	Mean	Bias	Std. Dev.	Number	Mean	Bias	Std. Dev.
2000	2.32	0.06	1.71	7840	1.85	−0.41	1.99
2001	2.58	−0.01	1.70	8480	1.79	−0.80	2.46
2002	2.76	0.01	2.17	5728	2.00	−0.76	3.14
2003	1.82	0.07	1.54	7552	1.47	−0.27	2.15
2004	2.46	0.00	1.81	9063	1.62	−0.83	2.77
2005	2.17	−0.06	1.84	8884	1.44	−0.78	2.79
All	2.34	0.01	1.79	47 547	1.68	−0.65	2.57

mean-field bias is present in the adjusted accumulation composites. In addition the standard deviation has been reduced and it is now substantially smaller than the mean precipitation depth. The number of gauge observations used for verification varies from year to year because only days where for each radar at least 280 reflectivity products are available in the archive have been included.

4.3. Verification against independent gauges

The results of the independent verification using the climatological gauge network are listed in Table II. Generally the results are similar to those in Table I but a few differences can be seen. The bias of the adjusted accumulations is not exactly zero, i.e. about 5% of the mean precipitation depth, for the independent verification. A verification of 13 climatological gauges against collocated (within 2.4 km) automatic gauges reveals a mean bias of +0.14 mm and a standard deviation of 1.14 mm thus explaining the observed bias of the adjusted composites against the independent dataset. Naturally the standard deviations of the accumulation composites against the independent rain gauge network are somewhat higher

Table II. Verification results for adjusted and raw accumulation composites against the independent dataset. The mean daily precipitation depth, bias, and standard deviation are listed in mm. The number of gauge observations used for the verification is listed as well.

	Adjusted				Raw		
Year	Mean	Bias	Std. Dev.	Number	Mean	Bias	Std. Dev.
2000	2.37	−0.03	1.95	80 510	1.88	−0.53	2.14
2001	2.63	−0.12	1.96	87 184	1.81	−0.93	2.58
2002	2.81	−0.10	2.39	58 891	2.02	−0.89	3.15
2003	1.86	−0.04	1.66	77 643	1.48	−0.43	2.16
2004	2.65	−0.23	2.21	64 394	1.70	−1.18	3.24
2005	2.35	−0.24	2.03	64 437	1.54	−1.05	3.03
All	2.43	−0.12	2.02	433 059	1.73	−0.82	2.72

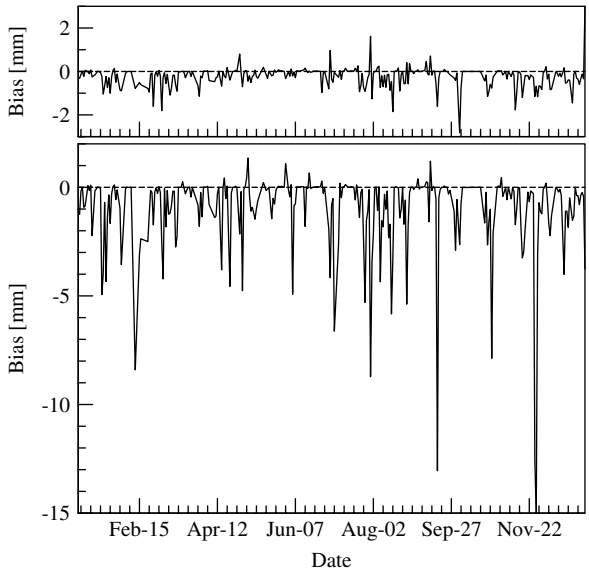

Figure 8. Mean-field bias time series of the adjusted (upper frame) and raw (lower frame) radar accumulations against the independent, climatological gauge network in 2005.

than those against the dependent network, but for the adjusted accumulations they are still substantially lower than the mean daily totals.

To relate the quality of radar accumulation products to meteorological circumstances, the mean-field bias and standard deviation have been calculated per day for 2005. Figure 8 shows the daily bias of the adjusted (upper frame) and raw (lower frame) radar accumulations with respect to the climatological gauge network. The largest underestimation of the raw radar accumulation is seen on 25–26 November 2005 which is the winter storm case used in Figures 2 and 4. It is evident that the mean underestimation is occasionally very substantial, i.e. 10 mm or more. In contrast, the daily bias of the adjusted accumulations is typically (much) smaller than 1 mm and hardly ever it is larger than that of the raw accumulations. So especially in cases of extreme underestimation by the raw radar products the bias-adjustment procedure has a large positive impact.

Figure 9 shows the biases (left frame) and standard deviations (right frame) of the bias-adjusted accumulation composites against the individual climatological rain gauges. The coloured dots in the maps indicate either the bias or the standard deviation for the underlying rain gauge. When we focus on the biases, slightly positive values (green dots) are seen in the central parts of The Netherlands and substantial underestimation (blue-purple) is seen in southwest, southeast, and northeast corners of The Netherlands. The clear outlier (red dot) marked with a circle is due to semi-permanent residual clutter from anomalous propagation of the Den Helder radar over the 'IJssel' lake. The values of the station biases and standard deviations should be related to the mean daily precipitation depth of 2.43 mm (Table II). The observed pattern is consistent with a slight overestimation at short range and a (substantial) underestimation

DOI: 10.1002/met

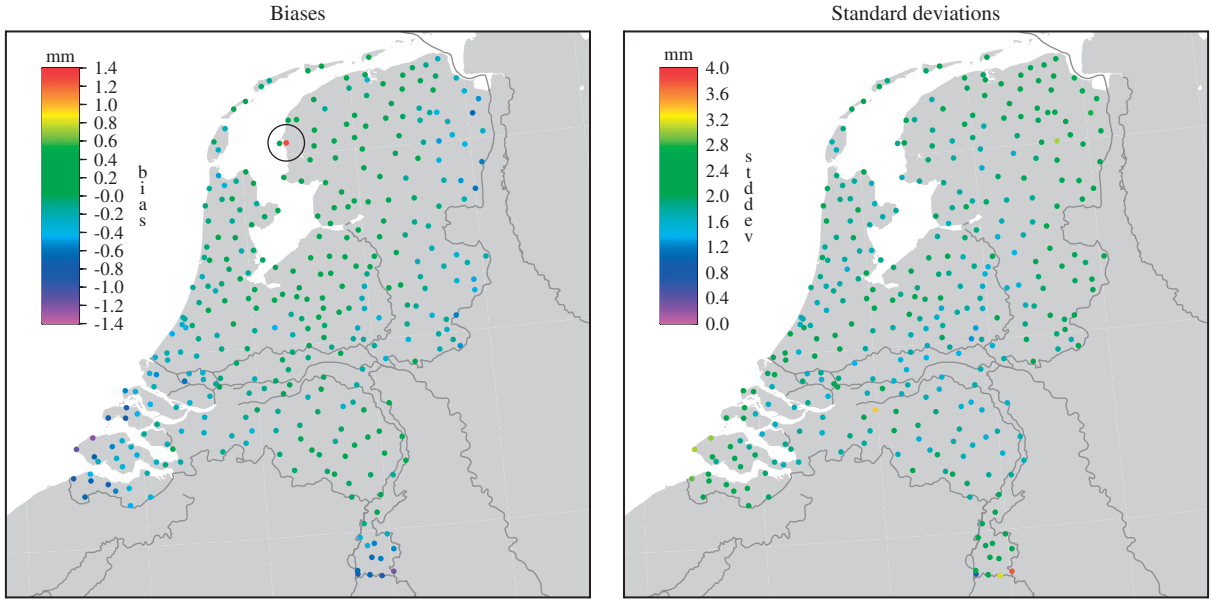

Figure 9. This figure shows two maps of the biases (left frame) and standard deviations (right frame) of the bias-adjusted accumulation composites against the climatological rain gauge network. Data from the whole verification period (2000–2005) have been used. Biases and standard deviations are given in mm. A clear outlier in the left frame (see text) is marked with a circle.

at long-range by the weather radars. Obviously the mean-field bias adjustment method cannot correct for this range dependency of the bias.

The right map with the standard deviations reveals an homogeneous distribution and only on the southern edge of The Netherlands a few high values are seen. The lowest standard deviations (blue dots) are seen in the southern part and western part of The Netherlands and somewhat higher values are seen in northeast, southwest and central parts of The Netherlands. The standard deviation of a radar-gauge comparison is largely due to representativeness errors, i.e. differences in the sampled volumes (Kitchen and Blackall, 1992).

5. Conclusions

The non-uniform VPR, the conversion of radar reflectivity Z to rainfall rate R, and the attenuation due to strong precipitation are the major sources of error in C-band radar quantitative precipitation estimation. Adjustment methods for non-uniform VPR are still topic of research and operational application is currently in its infancy. The impact of the last two sources of error can be reduced considerably by operation of a so-called dual polarization weather radar (Bringhi and Chandrasekar, 2001), but it will probably take another 10 years before KNMI will operate this type of radar. In this paper it has been demonstrated that the quality of the 3-h accumulation composites (updated hourly) can be significantly enhanced by a straightforward bias-adjustment procedure.

The quality of the bias-adjusted 3-h accumulation products has been evaluated using both dependent and independent gauge observations. A 6-year dataset of bias-adjusted accumulation products between 2000 and 2005 was used for the verification. It is concluded that the proposed scheme effectively removes the mean-field bias from the raw accumulation products and that it substantially reduces the daily standard deviation. The mean-field bias varies strongly from day-to-day depending on the weather conditions. From a spatial analysis it is concluded that the quality of the product degrades with increasing range. Therefore, it is recommended to develop a simple VPR adjustment procedure for correction of the range-dependent bias suited for operational implementation.

Acknowledgements

Daan Vogelezang and Aart Overeem (KNMI) are gratefully acknowledged for reviewing an earlier version of the manuscript. The skillful assistance of Siebren de Haan (KNMI) with the production of the figures is highly appreciated.

References

Andrieu H, Creutin JD. 1995. Identification of vertical profiles of radar reflectivity for hydrological applications using an inverse method. Part I: formulation. *Journal of Applied Meteorology* **34**: 225–239.

Berne A, Uijlenhoet R. 2006. Quantitative analysis of X-band weather radar attenuation correction accuracy. *Natural Hazards and Earth System Sciences* **6**: 419–425.

Borga M, Tonelli F, Moore RJ, Andrieu H. 2002. Long-term assessment of bias adjustment in radar rainfall estimation. *Water Resources Research* **38**: 1226.

Bringhi VN, Chandrasekar V. 2001. *Polarimetric Doppler Weather Radar*. Cambridge University Press: UK; 636.

Chumchean S, Sharma A, Seed A. 2006. An integrated approach to error correction for real-time radar-rainfall estimation. *Journal of Atmospheric and Oceanic Technology* **23**: 67–79.

Collier CG. 1983. A weather radar correction procedure for real-time estimation of surface rainfall. *Quarterly Journal of the Royal Meteorological Society* **109**: 589–608.

Collier CG. 1986a. Accuracy of rainfall estimates by radar, part I: calibration by telemetering raingauges. *Journal of Hydrology* **83**: 207–223.

DOI: 10.1002/met

Collier CG. 1986b. Accuracy of rainfall estimates by radar, part II: comparison with raingauge network. *Journal of Hydrology* **83**: 225–235.

Delrieu G, Hucke L, Creutin JD. 1999. Attenuation in rain for X-band and C-band weather radar systems: Sensitivity with respect to the drop size distribution. *Journal of Applied Meteorology* **38**: 57–68.

Fulton RA, Breidenbach JP, Sea D-J, Miller DA, O'Bannon T. 1998. The WSR-88D rainfall algorithm. *Weather and Forecasting* **13**: 377–395.

Gematronik. 2003. Rainbow 3.4 operator's manual, Gematronik GmbH., Raiffeneisenstr. 10, 41470 Neuss, Germany. Release 4.7.

Harrison DL, Driscoll SJ, Kitchen M. 2000. Improving precipitation estimates from weather radar using quality control and correction techniques. *Meteorological Applications* **6**: 135–144.

Hitschfeld W, Bordan J. 1954. Errors inherent in the radar measurement of rainfall at attenuating wavelengths. *Journal of Meteorology* **11**: 58–67.

Holleman I. 2004. VPR adjustment using a dual CAPPI technique. *ERAD Publication Series* **2**: 25–30.

Joss J, Waldvogel A. 1990. *Radar in Meteorology*. AMS: Boston, MA, chapter Precipitation Measurement and Hydrology; 577–606.

Kitchen M, Blackall RM. 1992. Representativeness errors in comparisons between radar and gauge measurements of rainfall. *Journal of Hydrology* **134**: 13–33.

Koistinen J. 1991. Operational correction of radar rainfall errors due to the vertical reflectivity profile. *25th Conference on Radar Meteorology*. American Meteorological Society: Paris; 91–94.

Koistinen J, Pohjola H, Hohti H. 2003. Vertical reflectivity profile classification and correction in radar composites in Finland. *31st Conference on Radar Meteorology*. American Meteorological Society: Seattle; 534–537.

Marshall JS, Hitschfeld W, Gunn KLS. 1955. Advances in radar weather. *Advances in Geophysics*, Vol. 2. Academic Press: New York; 1–56.

Marshall JS, Palmer WM. 1948. The distribution of raindrops with size. *Journal of the Atmospheric Sciences* **5**: 165–166.

Michelson DB, Jones CG, Landelius T, Collier CG, Haase G, Heen M. 2005. 'Down-to-Earth' modelling of equivalent surface precipitation using multisource data and radar. *Quarterly Journal of the Royal Meteorological Society* **131**: 1093–1112.

Rossa A, Bruen M, Macpherson B, Holleman I, Michelson D, Michaelides S (eds). 2005. *COST Action 717: Use of Radar Observations in Hydrology and NWP Models*, EU (Brussels). EUR 21954.

Sigmet. 1998. *RVP6 Doppler Signal Processor User's Manual*. Sigmet Inc.: 2 Park Drive, Westford, MA, 01886 USA. ROM Rev. 39.

Uijlenhoet R, Stricker JNM. 1999. A consistent rainfall parameterization based on the exponential raindrop size distribution. *Journal of Hydrology* **218**: 101–127.

Vignal B, Andrieu H, Creutin JD. 1999. Identification of vertical profiles of reflectivity from volume scan radar data. *Journal of Applied Meteorology* **38**: 1214–1228.

Vignal B, Galli G, Joss J, Germann U. 2000. Three methods to determine profiles of reflectivity from volumetric radar data to correct precipitation estimates. *Journal of Applied Meteorology* **39**: 1715–1726.

Vignal B, Krajewski W. 2001. Large-sample evaluation of two methods to correct range-dependent error for WSR-88D rainfall estimates. *Journal of Hydrometeorology* **2**: 490–504.

Wessels HRA, Beekhuis JH. 1994. Stepwise procedure for suppression of anomalous ground clutter. In COST−75• Seminar on Advanced Radar Systems, Brussels, Belgium; 270–277, EUR 16013 EN.

Wilson JW. 1970. Integration of radar and raingage data for improved rainfall measurement. *Journal of Applied Meteorology* **9**: 489–497.

Wilson JW, Brandes EA. 1979. Radar measurement of rainfall – a summary. *Bulletin of the American Meteorological Society* **60**: 1048–1058.

DOI: 10.1002/met